NASA TECHNICAL MEMORANDUM

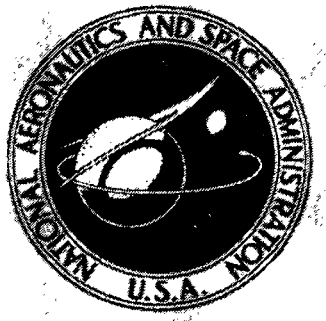

NASA TM X-2473

NASA TM X-2473

AERODYNAMIC CHARACTERISTICS OF AN OGEE-WING SPACE-SHUTTLE ORBITER CONCEPT AT A MACH NUMBER OF 2.01

by Lawrence E. Putnam

Langley Research Center
Hampton, Va. 23365

NATIONAL AERONAUTICS AND SPACE ADMINISTRATION • WASHINGTON, D. C. • FEBRUARY 1972

1. Report No.	2. Government Accession No.	3. Recipient's Catalog No.
NASA TM X-2473		

4. Title and Subtitle	5. Report Date
AERODYNAMIC CHARACTERISTICS OF AN OGEE-WING SPACE-SHUTTLE ORBITER CONCEPT AT A MACH NUMBER OF 2.01	February 1972
	6. Performing Organization Code
7. Author(s)	8. Performing Organization Report No.
Lawrence E. Putnam	L-8084
	10. Work Unit No.
9. Performing Organization Name and Address	117-07-01-01
NASA Langley Research Center Hampton, Va. 23365	11. Contract or Grant No.
	13. Type of Report and Period Covered
12. Sponsoring Agency Name and Address	Technical Memorandum
National Aeronautics and Space Administration Washington, D.C. 20546	14. Sponsoring Agency Code

15. Supplementary Notes

16. Abstract

An investigation has been made at a Mach number of 2.01 to determine the effects of a flared rudder on the aerodynamic characteristics of an ogee-wing space-shuttle orbiter configuration. Also investigated were the effects of an upper-aft fuselage fairing for the orbital maneuvering system, elevon deflections, and rudder deflection on the aerodynamic characteristics of the configuration.

17. Key Words (Suggested by Author(s))	18. Distribution Statement
Space shuttle orbiter Supersonic speeds Longitudinal, lateral, and directional characteristics	Unclassified – Unlimited

19. Security Classif. (of this report)	20. Security Classif. (of this page)	21. No. of Pages	22. Price*
Unclassified	Unclassified	30	$3.00

*For sale by the National Technical Information Service, Springfield, Virginia 22151

AERODYNAMIC CHARACTERISTICS OF AN OGEE-WING SPACE-SHUTTLE ORBITER CONCEPT AT A MACH NUMBER OF 2.01

By Lawrence E. Putnam
Langley Research Center

SUMMARY

An investigation has been made at a Mach number of 2.01 to determine the effects of a flared rudder on the aerodynamic characteristics of an ogee-wing space-shuttle orbiter configuration. Also investigated were the effects of an upper-aft fuselage fairing for the orbital maneuvering system, elevon deflection, and rudder deflection on the aerodynamic characteristics of the configuration.

The results of the investigation indicated that the flared rudder substantially increased the directional stability and the positive effective dihedral of the configuration. A rudder flare angle of 30° increased the directional stability of the basic configuration, which was directionally unstable at all test angles of attack (-4° to 27°), so that the orbiter was stable to an angle of attack of approximately 18°. The drag coefficient and pitching-moment coefficient of the configuration increased with increasing rudder flare angle. The orbital-maneuvering-system fairing increased the directional stability and the positive effective dihedral of the configuration at low angles of attack; above an angle of attack of 10°, there were only minor effects of the fairing. The fairing also increased the drag coefficient and pitching-moment coefficient of the configuration. A rudder deflection of 10° had only minor effects on the longitudinal aerodynamic characteristics of the configuration. An elevon deflection of -45° provides a sufficient pitching-moment increment to trim the configuration with orbital-maneuvering-system fairing on to an angle of attack of approximately 15°.

INTRODUCTION

The National Aeronautics and Space Administration is currently studying space-shuttle vehicle systems to provide economical earth to earth-orbit transportation for such missions as logistic support of space stations, satellite placement and inspection, space rescue, and earth-orbit insertion of payloads for missions beyond earth orbit. (See refs. 1 to 3.) Several two-stage space-shuttle configurations are being investigated.

Included in these investigations have been wind-tunnel tests to evaluate the aerodynamic characteristics of the proposed booster-orbiter configurations and the orbiter configurations alone. (See, for example, refs. 4 and 5.)

In general, the orbiter configurations developed during the aforementioned studies have blended wing bodies with the vertical tail located on the fuselage center line. The ogee wing for the configuration of the present investigation has a leading-edge sweep of 55° at the midsemispan of the wing. During the moderate supersonic speed part (Mach 1.6 to 2.4) of the reentry into the earth's atmosphere, this configuration will be at angles of attack from 10° to 20° where, in general, conventional delta-wing or ogee-wing configurations with center-line vertical tails lose directional stability. The present investigation was undertaken, therefore, to determine the effects of a flared rudder which was designed to improve the supersonic directional stability characteristics of the configuration. Also included in the present wind-tunnel investigation were tests to determine the effects of an upper-aft fuselage fairing for the orbital maneuvering system, elevon deflection, and rudder deflection.

The tests were made in the Langley 4- by 4-foot supersonic pressure tunnel at a Mach number of 2.01 and primarily at a Reynolds number, based on the wing reference chord, of 1.3×10^{6}. The angle of attack was varied from -4° to 27° at angles of sideslip of 0° and 5°.

SYMBOLS

The longitudinal force and moment coefficients are referenced to the body-axis system or the stability-axis system. The lateral and directional force and moment coefficients are referenced to the body-axis system. The origin of these axis systems is located at 67 percent of the fuselage length and at 41.4 percent of the fuselage maximum height. The symbols are defined as follows:

A	aspect ratio
b	wing span, 22.936 cm
$\bar{c}$	wing reference chord, 13.142 cm
C_A	axial-force coefficient, $\frac{\text{Axial force}}{qS}$
$C_{A,base}$	base axial-force coefficient

C_D drag coefficient, $\frac{\text{Drag}}{qS}$

$C_{D,f}$ skin-friction drag coefficient

$C_{D,o}$ drag coefficient at zero lift

C_L lift coefficient, $\frac{\text{Lift}}{qS}$

C_l rolling-moment coefficient, $\frac{\text{Rolling moment}}{qSb}$

C_{l_β} effective dihedral parameter, $\frac{\partial C_l}{\partial \beta}$, per degree

C_m pitching-moment coefficient, $\frac{\text{Pitching moment}}{qS\bar{c}}$

$(C_m)_{\alpha=0^o}$ pitching-moment coefficient at zero angle of attack

C_N normal-force coefficient, $\frac{\text{Normal force}}{qS}$

C_n yawing-moment coefficient, $\frac{\text{Yawing moment}}{qSb}$

C_{n_β} directional stability parameter, $\frac{\partial C_n}{\partial \beta}$, per degree

C_Y side-force coefficient, $\frac{\text{Side force}}{qS}$

C_{Y_β} side-force derivative, $\frac{\partial C_Y}{\partial \beta}$, per degree

L/D lift-drag ratio

$(L/D)_{max}$ maximum lift-drag ratio

q free-stream dynamic pressure

R Reynolds number based on $\bar{c}$

S wing reference area, 252.325 sq cm

S_r rudder area

S_v vertical-tail area

α angle of attack, degrees

β angle of sideslip, degrees

δ_e elevon angle, positive with trailing edge down, degrees

δ_{flare} flare angle of rudder, degrees

δ_r rudder angle, degrees

$\delta_1, \delta_2, \delta_3$ angles defined in figure 3(a), degrees

Abbreviations:

BL buttock line in centimeters

FS fuselage station in centimeters

OMS orbital maneuvering system

WL water line in centimeters

MODEL

A sketch of the 0.00683-scale model of the basic orbiter configuration is presented in figure 1. Cross-sectional views and details of the model are presented in figures 2 and 3 and photographs of the model are presented in figure 4. The basic configuration had a blended wing body with the vertical tail mounted on the fuselage center line. The ogee wing had a midsemispan leading-edge sweep of 55° and an aspect ratio of 2.08. (The aspect ratio is based on the wing reference area.) The wing had an NACA 0010-64 airfoil at BL 2.811 and an NACA 0012-64 airfoil at BL 9.372. Note that at BL 2.811, the chord of the airfoil is defined by the theoretical wing planform shown in figure 1. Details of the strake ahead of the theoretical wing planform can be ascertained from the model cross sections in figure 2. The elevon located on the wing could be deflected from 0° to -45°. Details of the vertical tail and rudder are presented in figure 3(a). Interchangeable rudders with flare angles of 0°, 15°, and 30° were available for attachment

to the vertical tail. Provisions were made to deflect these rudders 10°. Shown in figures 3(b) and 4(b) is the fairing for the orbital maneuvering system.

APPARATUS AND PROCEDURES

Wind Tunnel and Instrumentation

The tests were made in the Langley 4- by 4-foot supersonic pressure tunnel. This wind tunnel is a continuous-flow single-return pressure tunnel with flexible top and bottom walls for changing nozzle contours. Tests can be made at Mach numbers from 1.41 to 2.20 at stagnation pressures from approximately 28 kN/m^2 to 207 kN/m^2 (0.276 to 2.043 atmospheres) and at a stagnation temperature of approximately 317 K. The dewpoint temperature of the tunnel is held at 244 K or less to avoid condensation.

The model was mounted on a six-component strain-gage balance which was sting supported in the wind tunnel. Pressure orifices were located at the base of the model and in the sting cavity to measure the base pressures on the configuration.

Tests

The investigation was conducted at a Mach number of 2.01, a stagnation temperature of 317 K, and primarily at a stagnation pressure of 87.36 kN/m^2 with a corresponding Reynolds number, based on the wing reference chord, of 1.3×10^6. Some limited tests (at an angle of attack for zero normal force) were made at stagnation pressures that varied from 13.47 kN/m^2 to 137.67 kN/m^2 with corresponding Reynolds numbers, based on wing reference chord, of 2.09×10^5 to 2.02×10^6. The angle of attack was varied from -4° to 27° at angles of sideslip of 0° and 5°. Some limited tests were made at angles of sideslip from -2° to 2° at an angle of attack of 0°.

The model was tested with the orbital-maneuvering-system fairing off and on. Tests were made with the flared rudder at 0°, 15°, and 30°. In general, the elevons were at 0° and the rudder was at 0°. However, some tests were made with the elevons at -45° and some tests were made with the rudder at 10°.

Boundary-Layer Transition

In general, the present investigation was made with fixed boundary-layer transition in order to minimize changes in the aerodynamic forces and moments due to change in the extent of laminar flow on the model. Some limited tests were made without transition strips to assess the effects of the transition strips on the drag characteristics of the configuration. Transition strips, 0.13 centimeter wide, were located on both sides of the vertical tail, on the top and bottom of the wing, and on the fuselage nose. (See fig. 5 for the location of these transition strips on the model.) The transition strips consisted

of 0.012-cm to 0.015-cm silicon carbide grains on the vertical tail, 0.015-cm to 0.018-cm silicon carbide grains on the wing, and 0.010-cm to 0.012-cm silicon carbide grains on the fuselage. The grain size and location of the transition strips were selected according to the recommendations of references 6 and 7. However, the transition strips on the vertical tail were placed further forward than the recommendations of reference 7 in order to locate the transition strips ahead of the rudder hinge line.

Corrections

The angle of attack and the angle of sideslip have been corrected for sting and balance deflections due to aerodynamic loads and for tunnel airstream angularity. The comparison of the data obtained with the model upright and with the model inverted, shown in figure 6, indicates the repeatability of the data.

The drag data represent gross drag in that base drag is included. Since the orbiter configuration will be in gliding unpowered flight at a Mach number of 2.01, these uncorrected data should be of more interest. However, the base axial-force data for each configuration are presented with the body-axis force and moment data. (The base area of the fuselage is 18.968 cm^2.)

RESULTS AND DISCUSSION

Effects of Reynolds Number

The effect of Reynolds number on the drag coefficient at zero lift for the configuration with and without transition strips is shown in figure 7. Also shown in this figure are theoretical estimates of the drag levels for a fully laminar, a fully turbulent, and a mixed boundary layer. The transition location for the mixed boundary layer was assumed to be at the transition strips on the model. The variation in turbulent-skin-friction drag was estimated by means of the Kármán-Schoenherr incompressible formula and the Sommer and Short T' method. (See ref. 8.) The variation in laminar-skin-friction drag was estimated by the Chapman-Rubesin formula. (See ref. 9.) For all boundary-layer conditions, the wave-drag coefficient was assumed to be 0.0465. For the configuration without transition strips, natural transition began to occur on the model at a Reynolds number, based on wing reference chord, of approximately 10^6. It appears that the grit selected for the transition strips on the model was not large enough to promote transition at the transition strip at the primary test Reynolds number. (The difference in the measured drag coefficient with transition fixed and with transition free is less than the theoretical estimates at $R = 1.3 \times 10^6$.) This deficiency in grit size should not affect any variable other than the drag coefficient of the configuration. (See ref. 10.)

Effects of Orbital-Maneuvering-System Fairing

The effects of the fairing for the orbital maneuvering system (OMS) on the longitudinal, lateral, and directional characteristics of the configuration are shown in figure 8. The addition of the fairing caused an increase in the pitching-moment coefficient but did not affect the longitudinal stability of the configuration. The fairing also decreased the normal-force coefficient and lift coefficient at a given angle of attack without changing their variation with angle of attack. An increase in drag coefficient and a corresponding reduction in lift-drag ratio also resulted from the addition of the OMS fairing. The increments in the longitudinal characteristics due to the orbital-maneuvering-system fairing were not significantly affected by increasing the rudder flare angles to 30°.

The OMS fairing increased the directional stability and the positive effective dihedral of the configuration at low angles of attack (fig. 8(c)) but had only minor effects at angles of attack greater than 10°. (It should be noted that the lateral and directional stability derivatives, C_{l_β}, C_{n_β}, and C_{Y_β}, were calculated from increments obtained between angles of sideslip of 0° and 5° and therefore do not account for any nonlinearities which may exist in the intermediate angle-of-sideslip range.) Flaring the rudder 30° does not significantly alter the effects of the OMS fairing on the lateral and directional aerodynamic characteristics of the configuration.

Effects of Flared Rudder

The effects of the flared rudder on the aerodynamic characteristics of the configuration with and without the OMS fairing are presented in figures 9 and 10, respectively. A summary of the effects of the flared rudder on various aerodynamic parameters is presented in figure 11. Increasing the rudder flare angle caused an increase in the pitching-moment coefficient at an angle of attack of 0° and the drag coefficient at zero lift and a reduction in maximum lift-drag ratio. There was essentially no effect of rudder flare angle on the longitudinal stability or on the lift characteristics of the orbiter configuration.

Flaring the rudder substantially increased the directional stability of the configuration. The basic configuration (OMS fairing off) was directionally unstable at all test angles of attack with $\delta_{flare} = 0^{\circ}$; however, the configuration was stable to angles of attack of approximately 18° with the rudder flared 30°. (See figs. 9(c) and 11.) The flared rudder also increased the positive effective dihedral of the configuration. At an angle of attack of 0° the variation of C_{n_β} and C_{l_β} with rudder flare angle was not essentially affected by the presence of the orbital-maneuvering-system fairing. However, the configuration with the OMS fairing was stable to higher angles of attack than the configuration without the fairing except at rudder flare angles near 30°.

Effects of Elevon Deflection

The effects of an elevon deflection of -45° on the longitudinal aerodynamic characteristics of the configuration with the orbital-maneuvering-system fairing and the rudder at a flare angle of 30° is presented in figure 10. The elevon effectiveness $\frac{\partial C_m}{\partial \delta_e}$ decreased slightly with increasing angle of attack. This configuration had sufficient elevon effectiveness to trim the configuration to the maximum test angle of attack, approximately 27°, with less than an elevon deflection of -45°. Applying the same elevon effectiveness to the configuration with no rudder flare indicated that this configuration can be trimmed to an angle of attack of approximately 15° with $\delta_e = -45^{\circ}$. The elevon deflection increased the drag coefficient and decreased the lift coefficient so that the maximum lift-drag ratio was reduced 27 percent.

Effects of Rudder Deflection

The effects of rudder deflection on the longitudinal aerodynamic characteristics of the configuration with the orbital-maneuvering-system fairing are presented in figure 12. There are only minor effects of a rudder deflection of 10° on the aerodynamic characteristics of the configuration with the rudder flare angle of zero. A comparison of the data of figure 10 for the configuration with $\delta_{flare} = 30^{\circ}$ and $\delta_r = 0^{\circ}$ with the data of figure 12 also shows that rudder deflection only had minor effects on the aerodynamic characteristics of the configuration with $\delta_{flare} = 30^{\circ}$.

CONCLUSIONS

An investigation has been made at a Mach number of 2.01 to determine the effects of a flared rudder on the aerodynamic characteristics of an ogee-wing space-shuttle orbiter configuration. Also investigated were the effects of an upper-aft fuselage fairing for the orbital maneuvering system, elevon deflection, and rudder deflection on the aerodynamic characteristics of the configuration. The results of the investigation indicate the following:

1. The flared rudder substantially increased the directional stability and the positive effective dihedral of the configuration. The basic configuration was directionally unstable at all test angles of attack (-4° to 27°); however, a rudder flare angle of 30° increased the directional stability such that the configuration was stable to an angle of attack of approximately 18°. The flared rudder increased the pitching-moment coefficient at zero angle of attack, increased the drag coefficient, and reduced the maximum lift-drag ratio.

2. The orbital-maneuvering-system fairing increased the directional stability and the positive effective dihedral at low angles of attack but had only minor effects at angles of attack greater than 10°. The fairing also increased the pitching-moment coefficient at zero angle of attack, increased the drag coefficient, and reduced the maximum lift-drag ratio.

3. A rudder deflection of 10° had only minor effects on the longitudinal aerodynamic characteristics of the configuration.

4. An elevon deflection of -45° provided a sufficient pitching-moment increment to trim the configuration with the orbital-maneuvering-system fairing and a rudder flare angle of 0° to an angle of attack of 15° and the configuration with a rudder flare angle of 30°, to the maximum test angle of attack of approximately 27°.

Langley Research Center,
National Aeronautics and Space Administration,
Hampton, Va., December 22, 1971.

REFERENCES

1. Mueller, George E.: The New Future for Manned Spacecraft Developments. Astronaut. & Aeronaut., vol. 7, no. 3, Mar. 1969, pp. 24-32.

2. Tischler, A. O.: A Commentary on Low-Cost Space Transportation. Astronaut. & Aeronaut., vol. 7, no. 8, Aug. 1969, pp. 50-64.

3. Mueller, George E.: An Integrated Space Program for the Next Generation. Astronaut. & Aeronaut., vol. 8, no. 1, Jan. 1970, pp. 30-51.

4. Fox, Charles H., Jr.; and Freeman, Delma C., Jr.: Subsonic Stability, Control, and Performance of a Shuttle Concept With a Blended Wing-Body. NASA TM X-2341, 1971.

5. Freeman, Delma C., Jr.: Low-Subsonic Aerodynamic Characteristics of a Space Shuttle-Orbiter Concept With a Blended Wing-Body. NASA TM X-2209, 1971.

6. Braslow, Albert L.; and Knox, Eugene L.: Simplified Method for Determination of Critical Height of Distributed Roughness Particles for Boundary-Layer Transition at Mach Numbers From 0 to 5. NACA TN 4363, 1958.

7. Braslow, Albert L.; Hicks, Raymond M.; and Harris, Roy V., Jr.: Use of Grit-Type Boundary-Layer-Transition Trips on Wind-Tunnel Models. NASA TN D-3579, 1966.

8. Sommer, Simon C.; and Short, Barbara J.: Free-Flight Measurements of Turbulent-Boundary-Layer Skin Friction in the Presence of Severe Aerodynamic Heating at Mach Numbers From 2.8 to 7.0. NACA TN 3391, 1955.

9. Chapman, Dean R.; and Rubesin, Morris W.: Temperature and Velocity Profiles in the Compressible Laminar Boundary Layer With Arbitrary Distribution of Surface Temperature. Jour. Aeronaut. Sci., vol. 16, no. 9, Sept. 1949, pp. 547-565.

10. Harris, Roy V.: Effects of Distributed Roughness Height on Aerodynamic Characteristics and Boundary-Layer Transition of a Wing-Body-Tail Configuration at a Mach Number of 1.61. NASA TN D-2334, 1964.

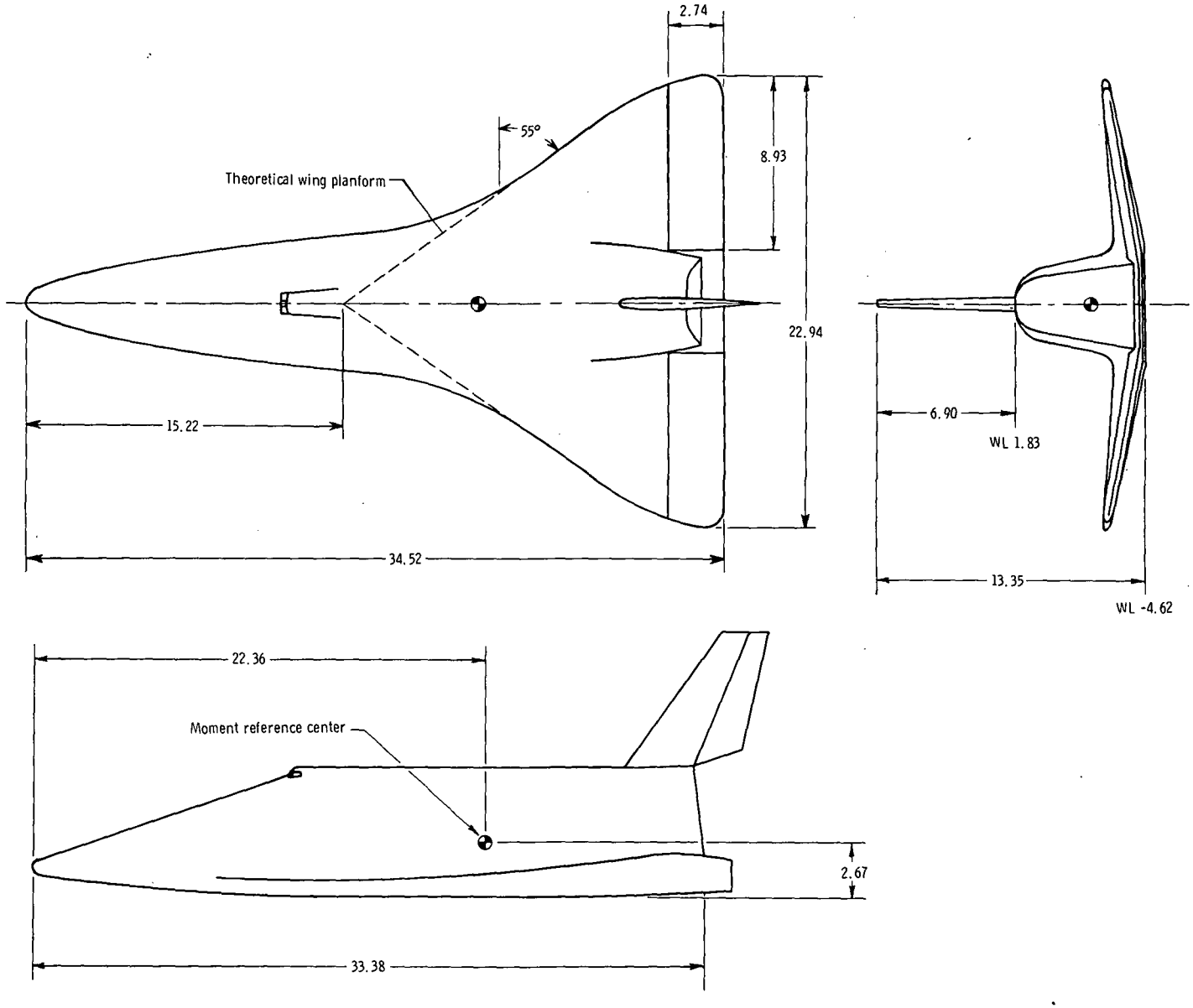

Figure 1.- Three-view drawing of basic model. All dimensions are in centimeters unless otherwise noted.

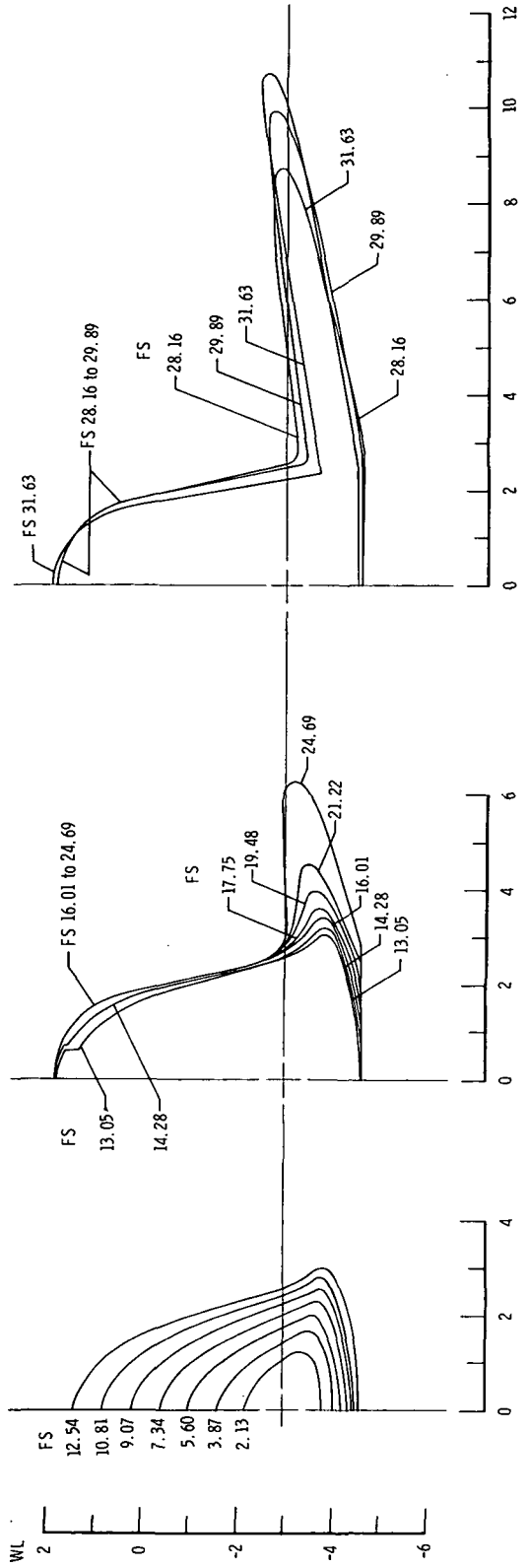

Figure 2.- Cross sections of the model. All dimensions are in centimeters unless otherwise noted.

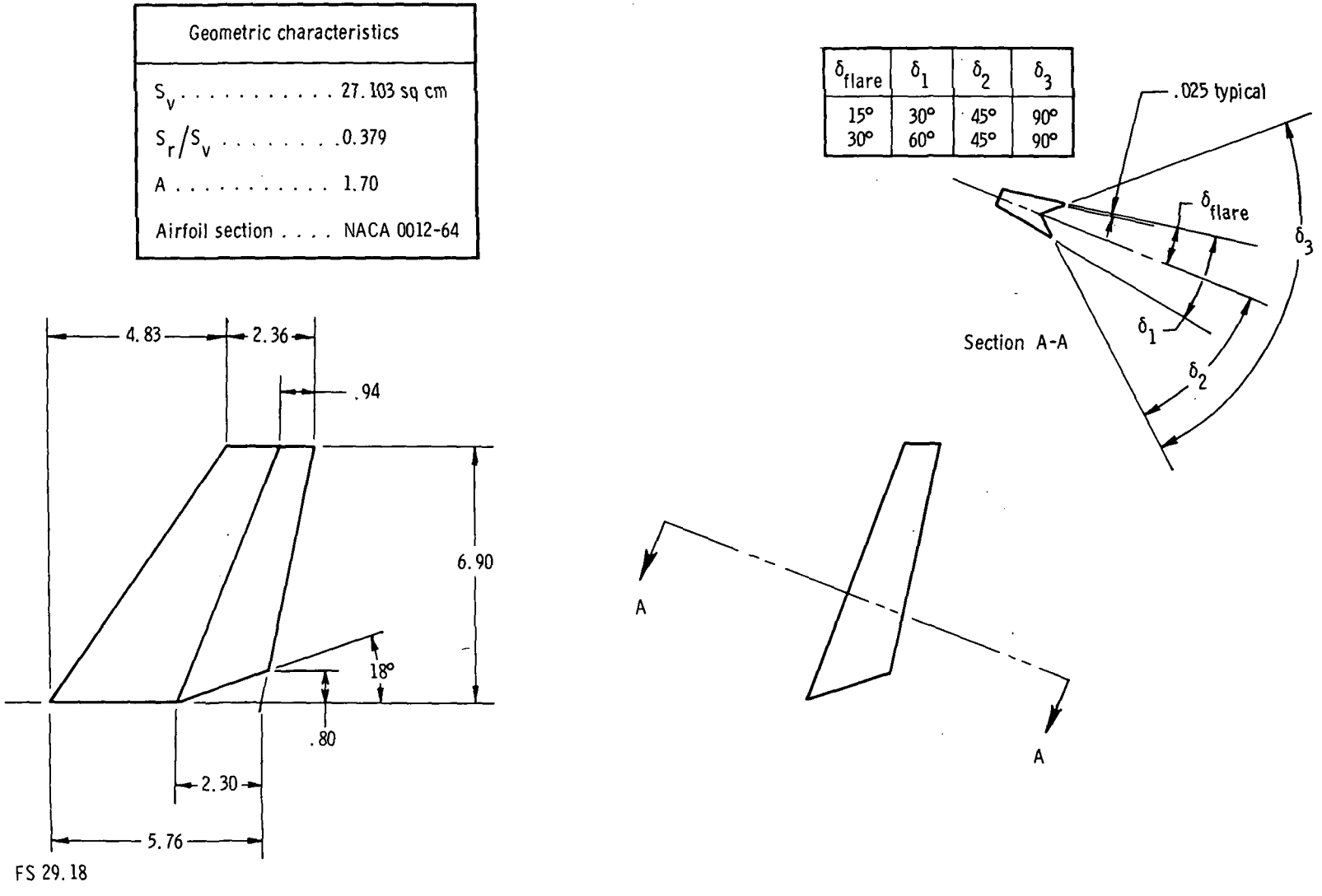

(a) Vertical tail and flared rudder.

Figure 3.- Details of model components. All dimensions are in centimeters unless otherwise noted.

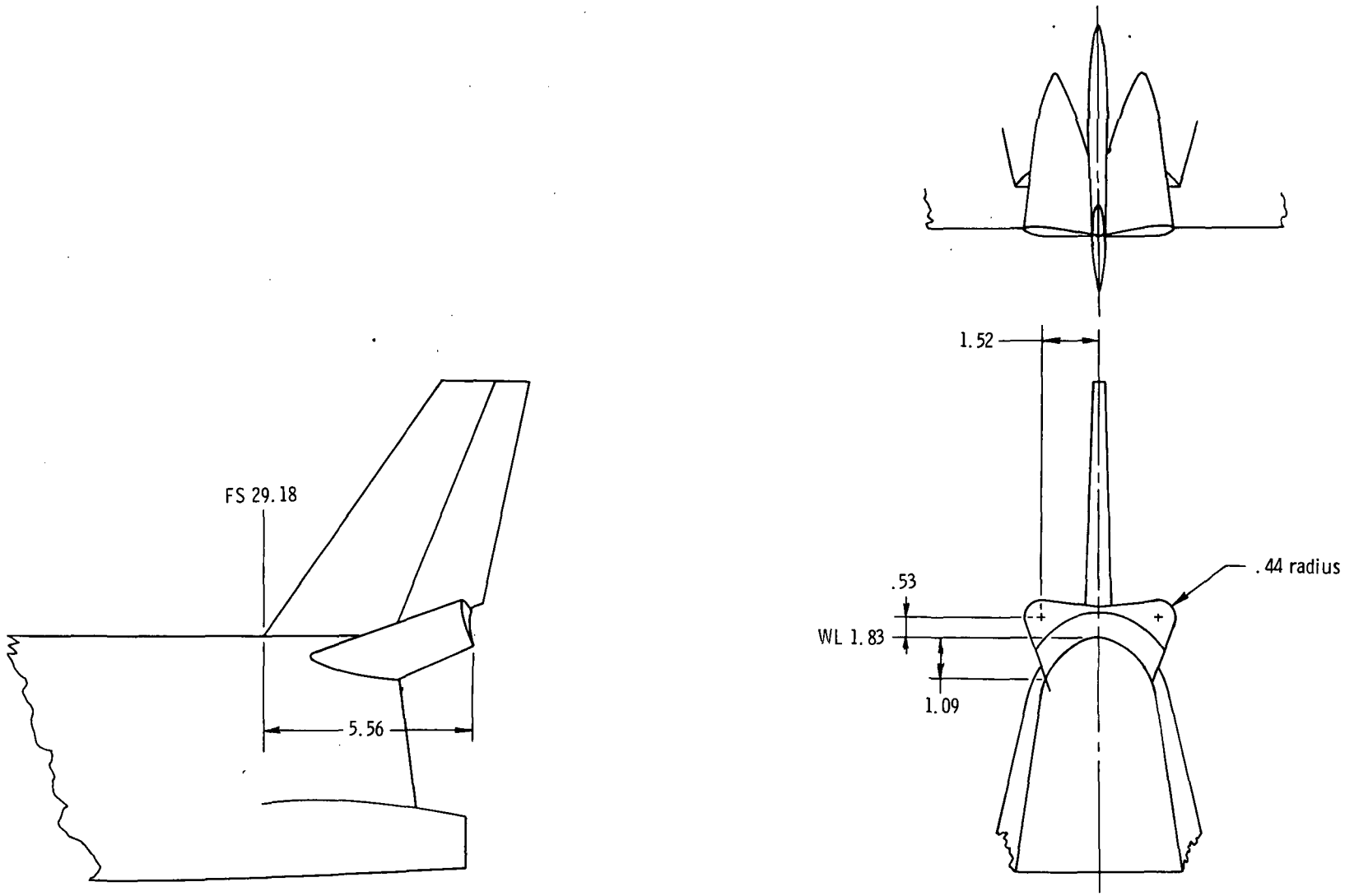

(b) Orbital-maneuvering-system fairing.

Figure 3.- Concluded.

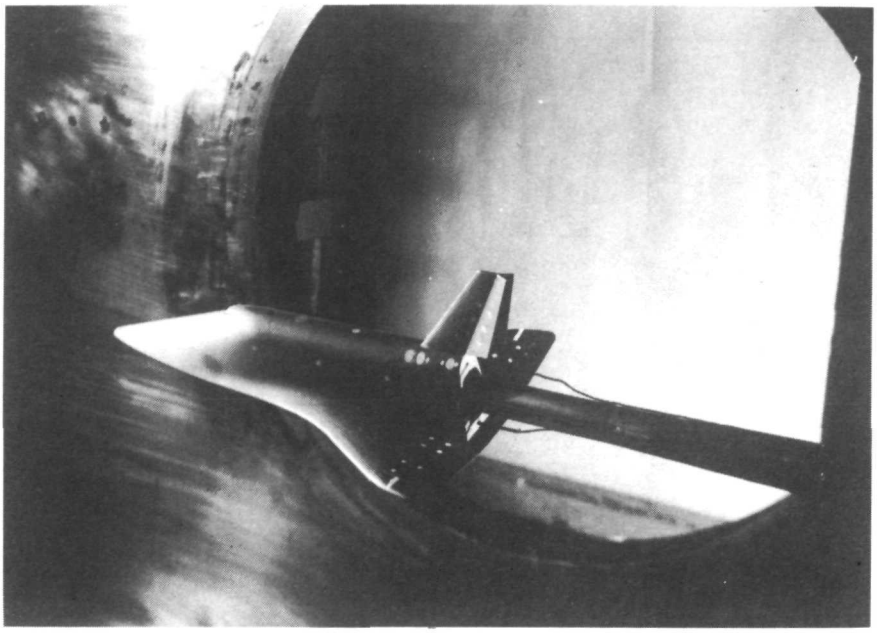

L-71-6303

(a) Configuration without orbital-maneuvering-system fairing.

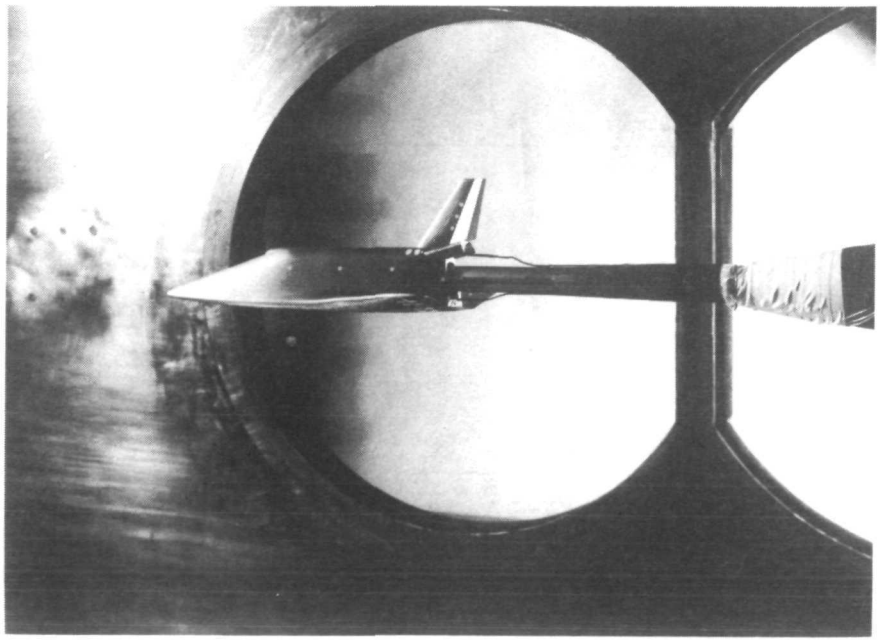

L-71-6302

(b) Configuration with orbital-maneuvering-system fairing.

Figure 4.- Photographs of model with $\delta_{flare} = 30^{o}$, $\delta_{r} = 0^{o}$, and $\delta_{e} = 0^{o}$.

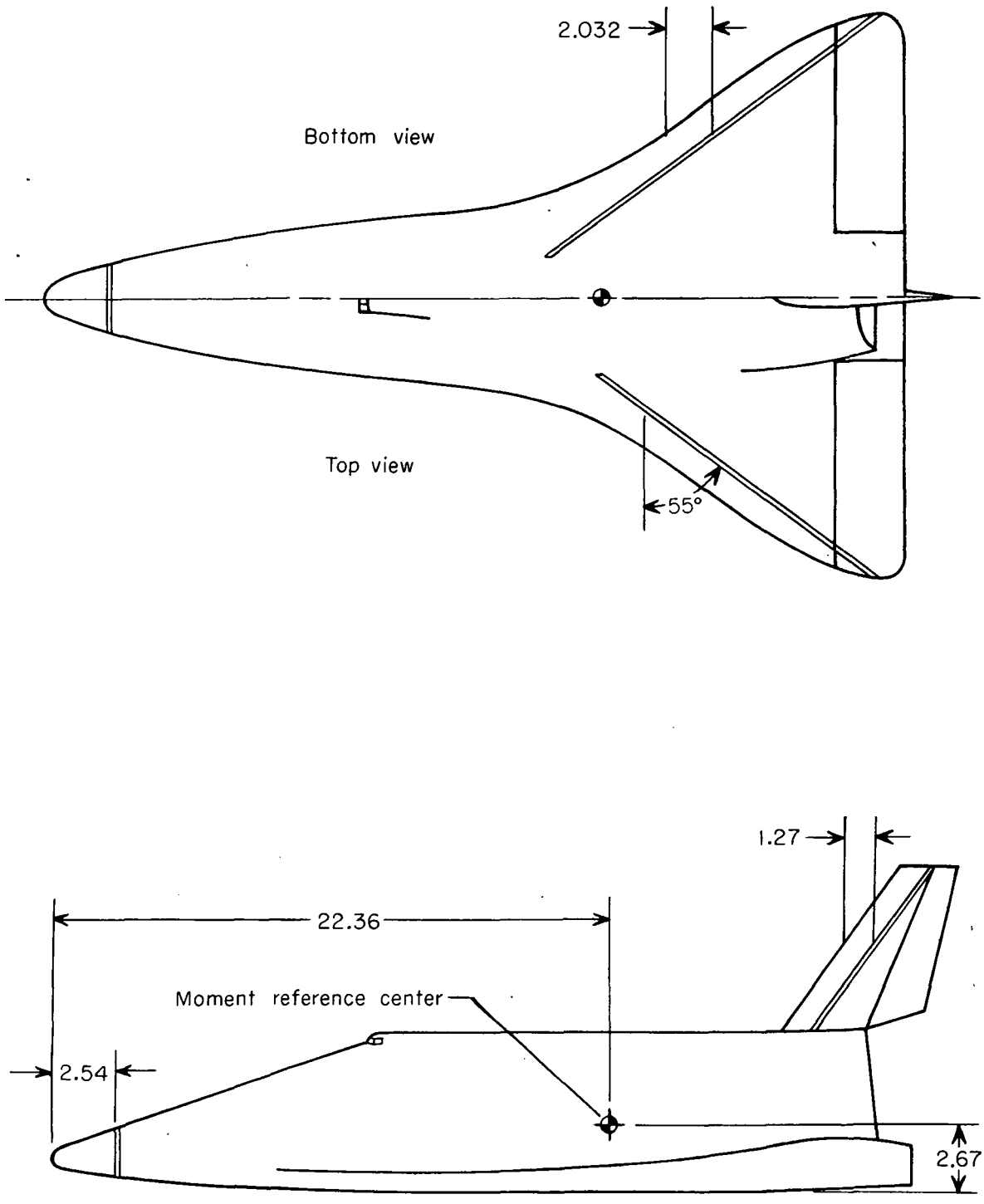

Figure 5.- Location of transition strips on the model. All dimensions are in centimeters unless otherwise noted.

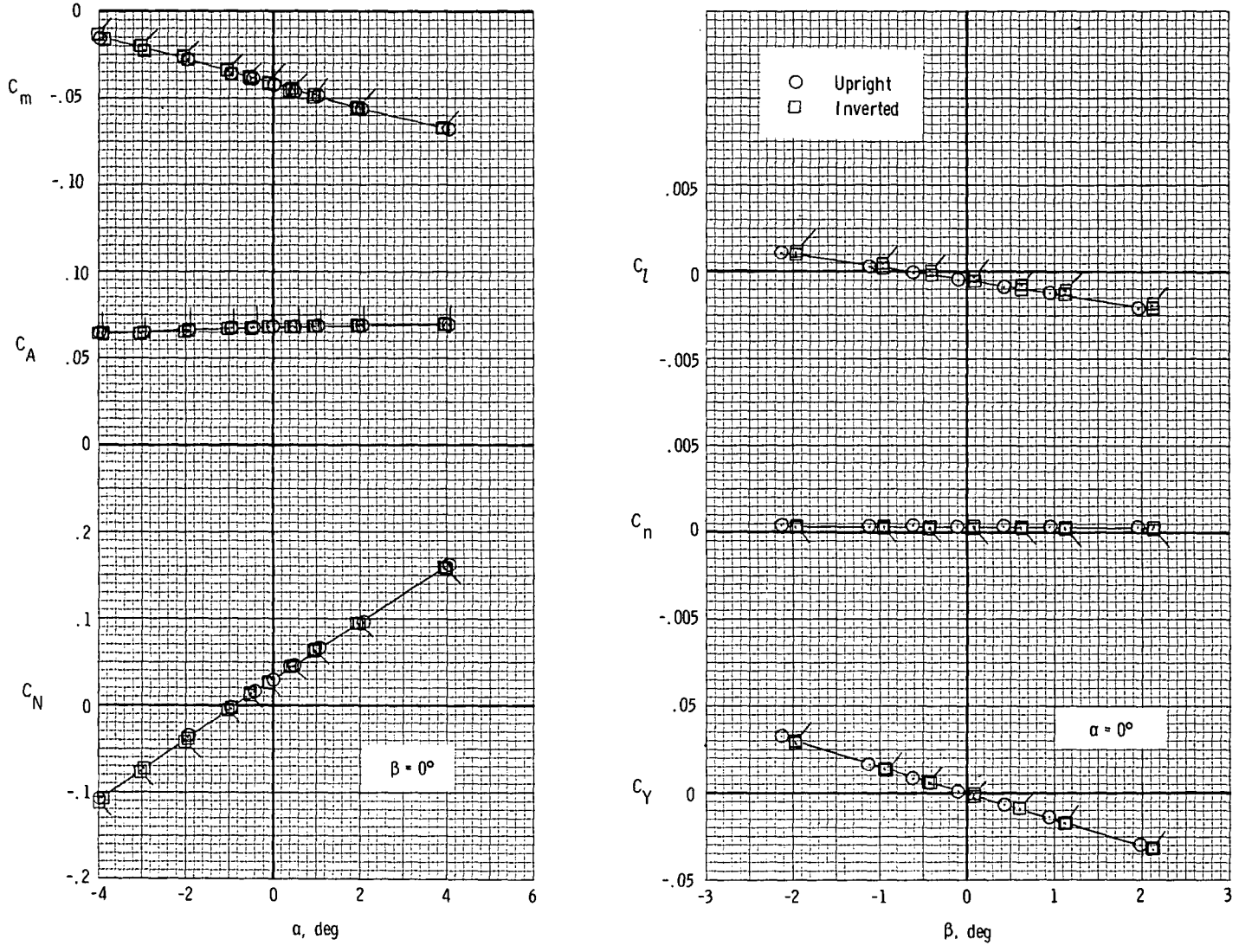

Figure 6.- Comparison of body-axis data obtained with the model upright and inverted. The configuration has the orbital-maneuvering-system fairing off, $\delta_{flare} = 0^o$, $\delta_r = 0^o$, and $\delta_e = 0^o$. (Flagged symbols indicate repeat data.)

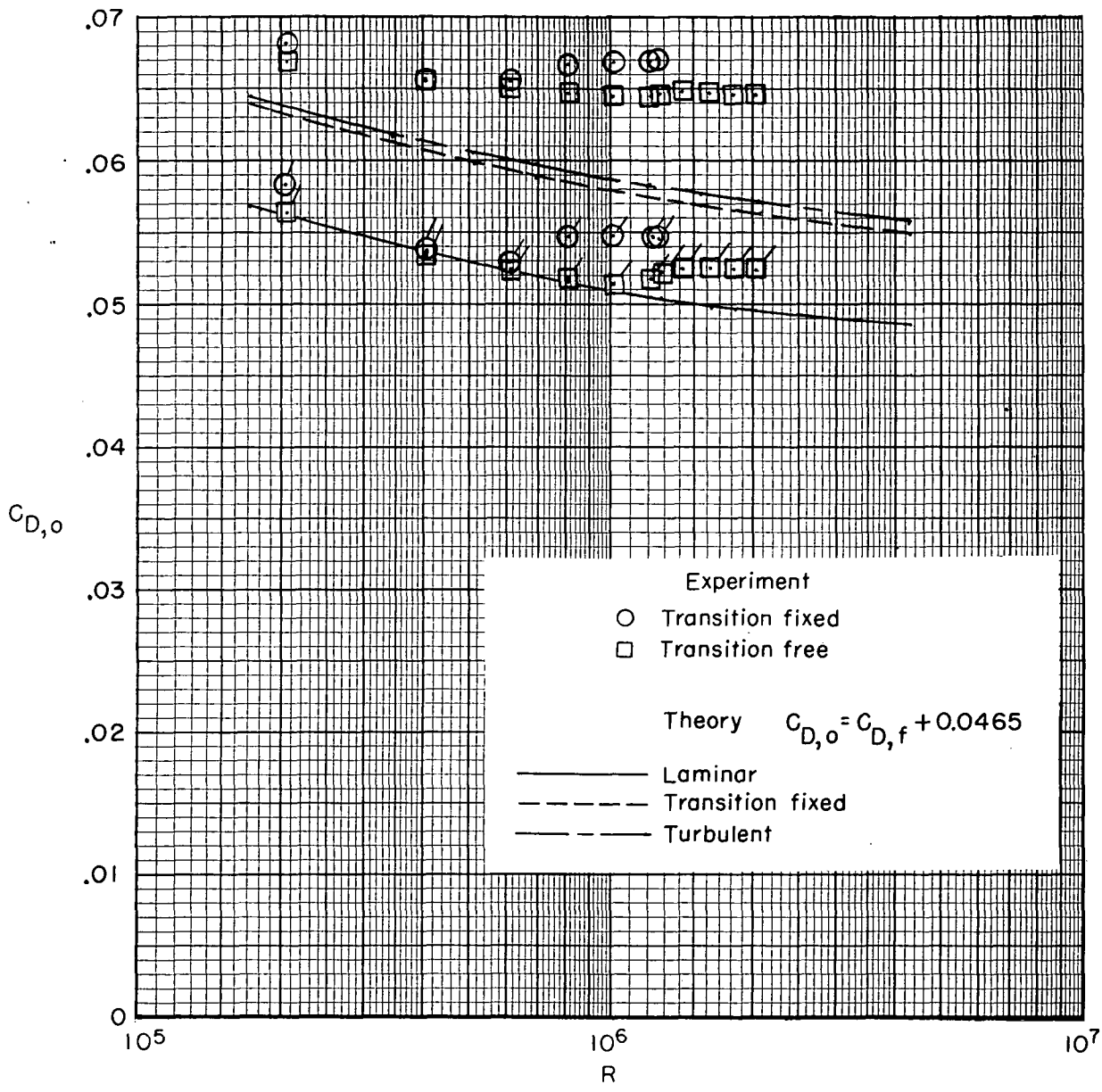

Figure 7.- Variation of drag coefficient at zero lift with Reynolds number for configuration without the orbital-maneuvering-system fairing. $\delta_{flare} = 0^o$; $\delta_r = 0^o$; and $\delta_e = 0^o$. Flagged symbols denote data corrected for base drag.

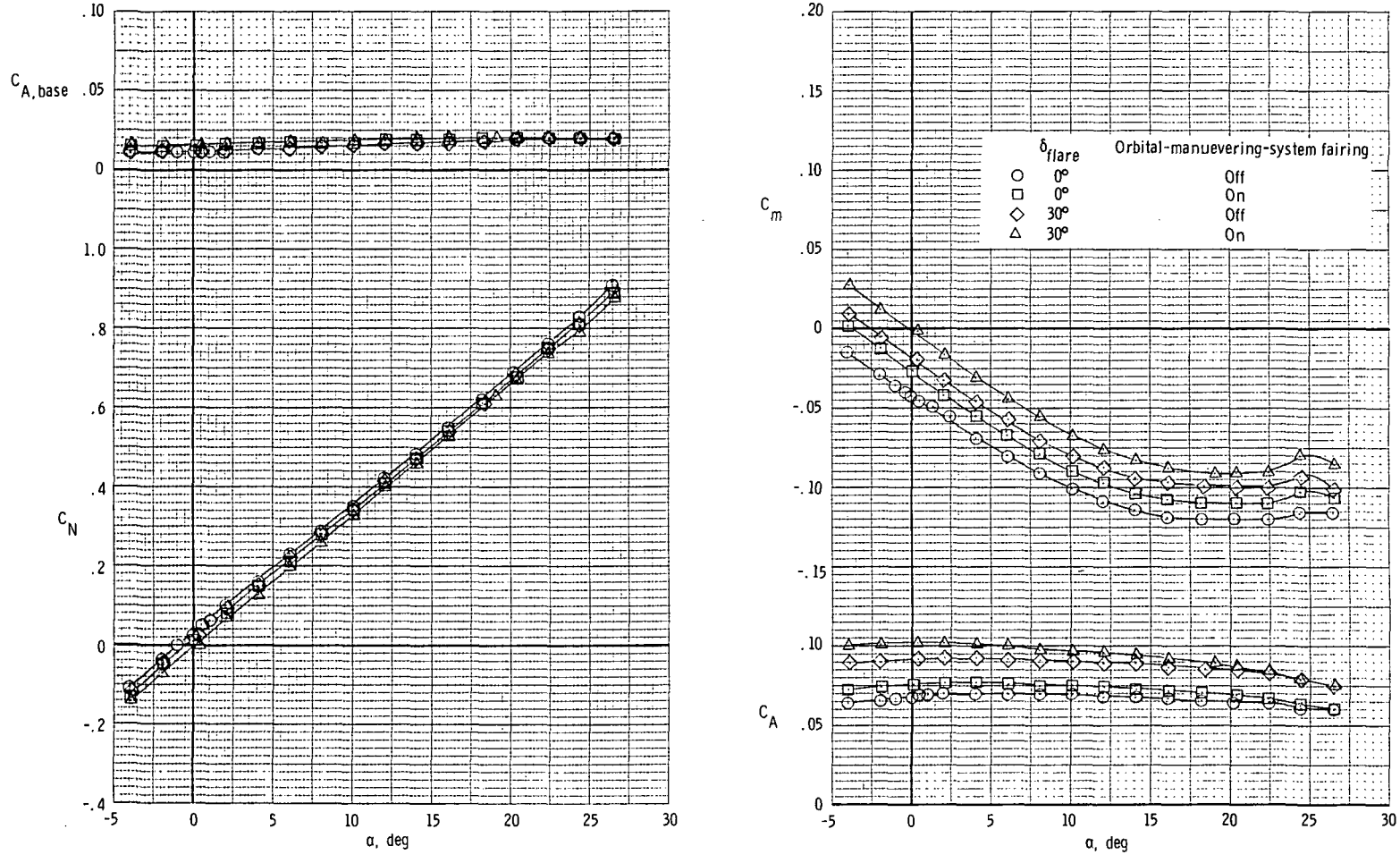

(a) Body-axis data.

Figure 8.- Effects of the orbital-maneuvering-system fairing on the aerodynamic characteristics of the configuration with $\delta_e = 0^o$ and $\delta_r = 0^o$.

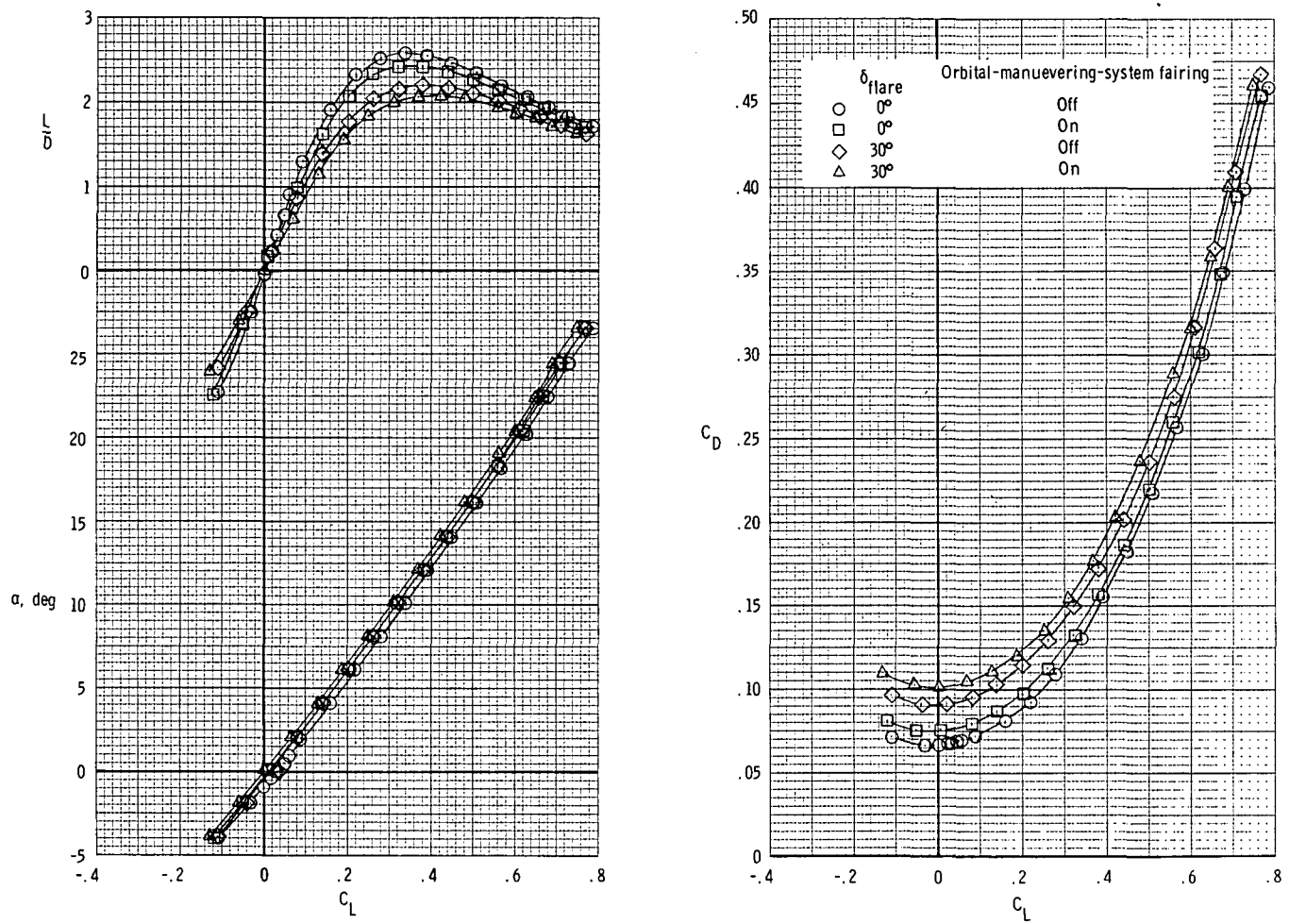

(b) Stability-axis data.

Figure 8.- Continued.

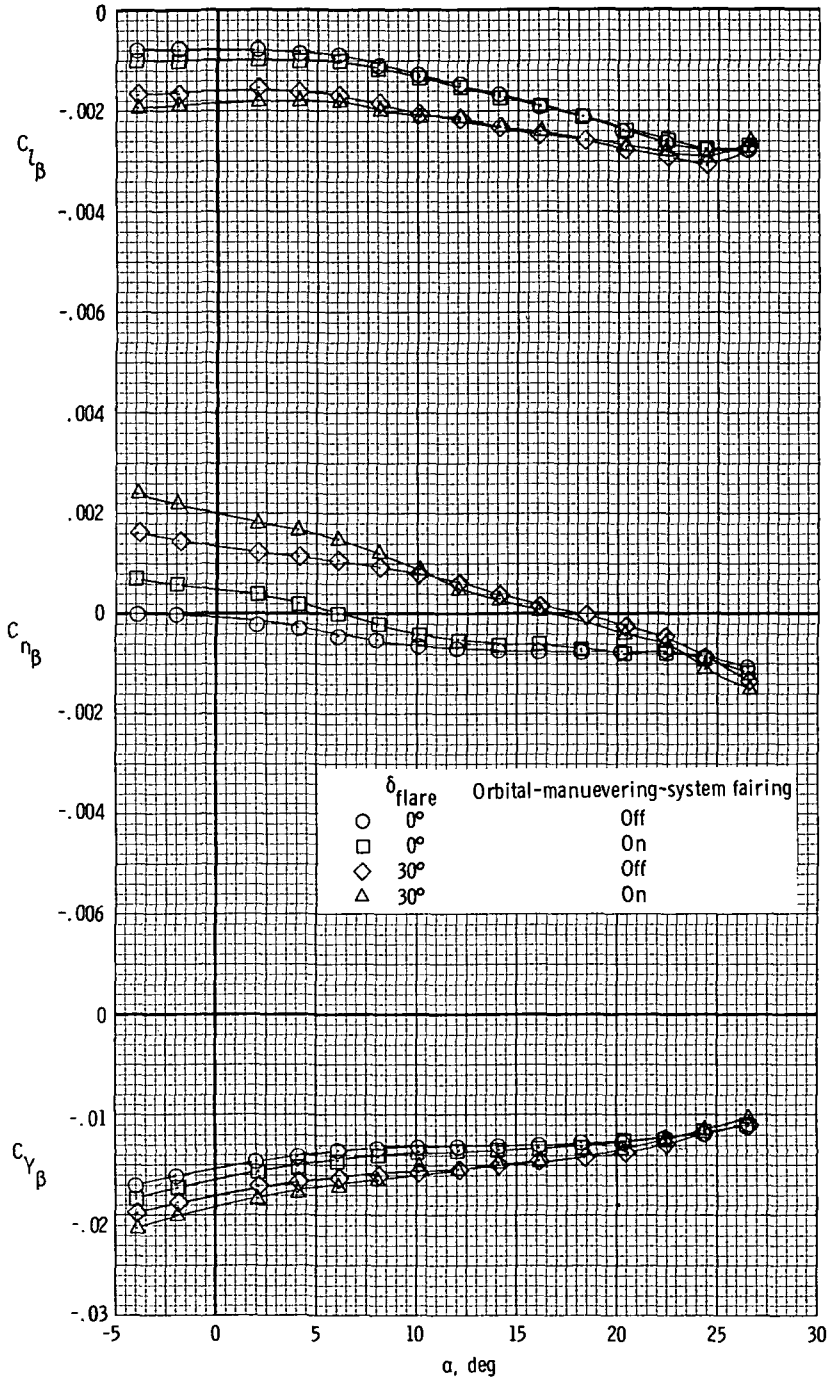

(c) Lateral and directional stability derivatives.

Figure 8.- Concluded.

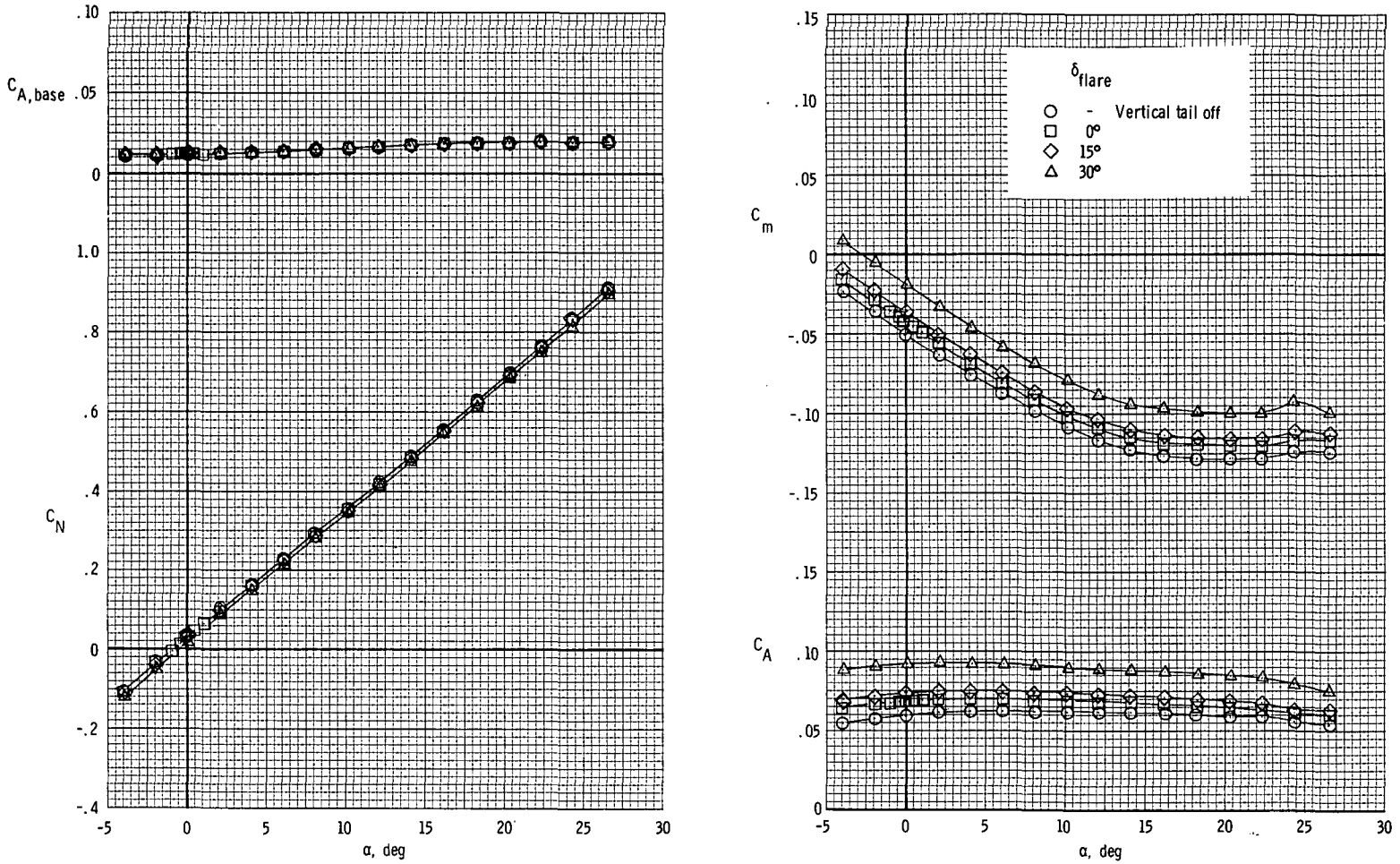

(a) Body-axis data.

Figure 9.- Effects of the flared rudder on the aerodynamic characteristics of the configuration without the orbital-maneuvering-system fairing and with $\delta_e = 0^o$ and $\delta_r = 0^o$.

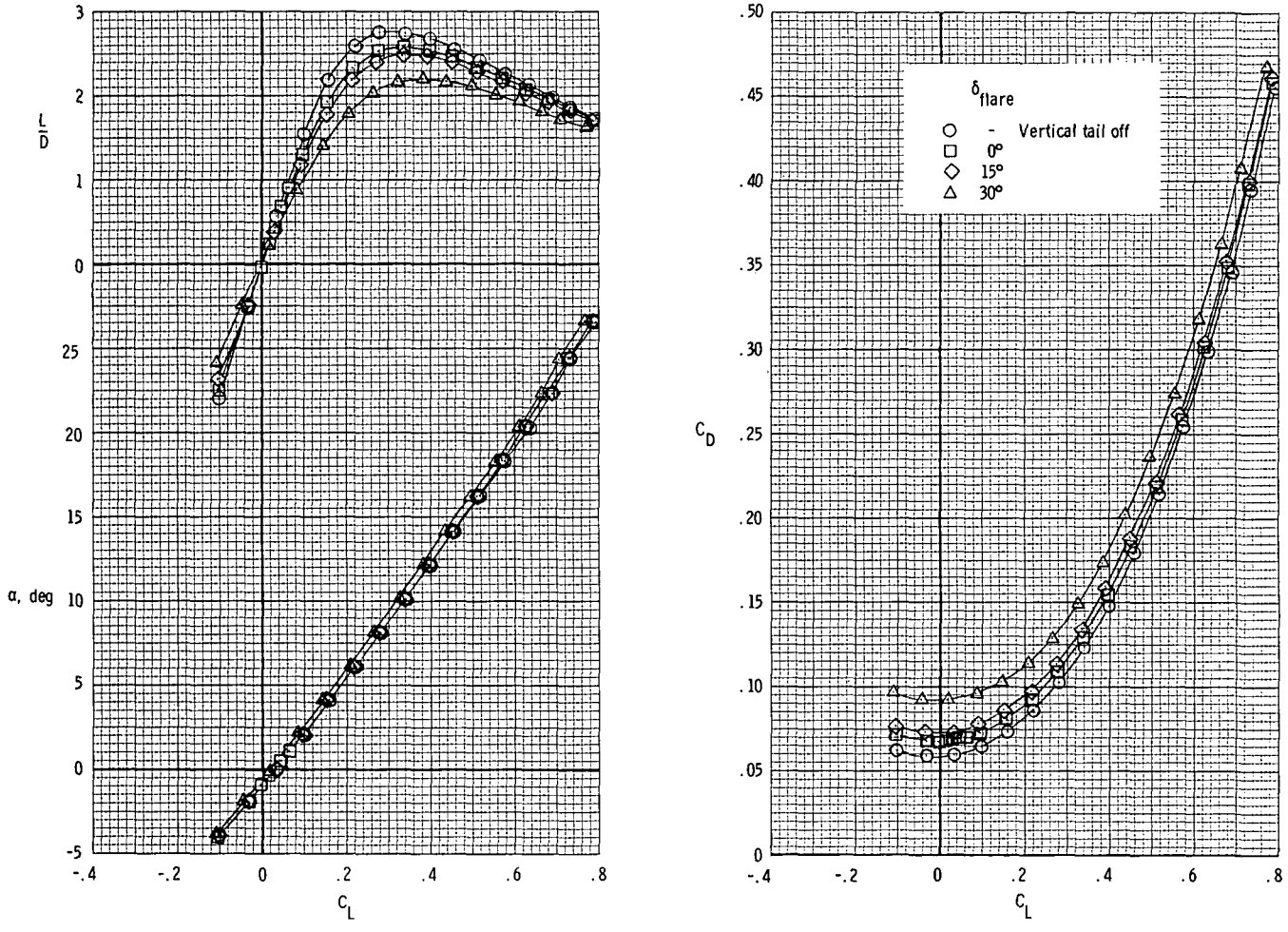

(b) Stability-axis data.

Figure 9.- Continued.

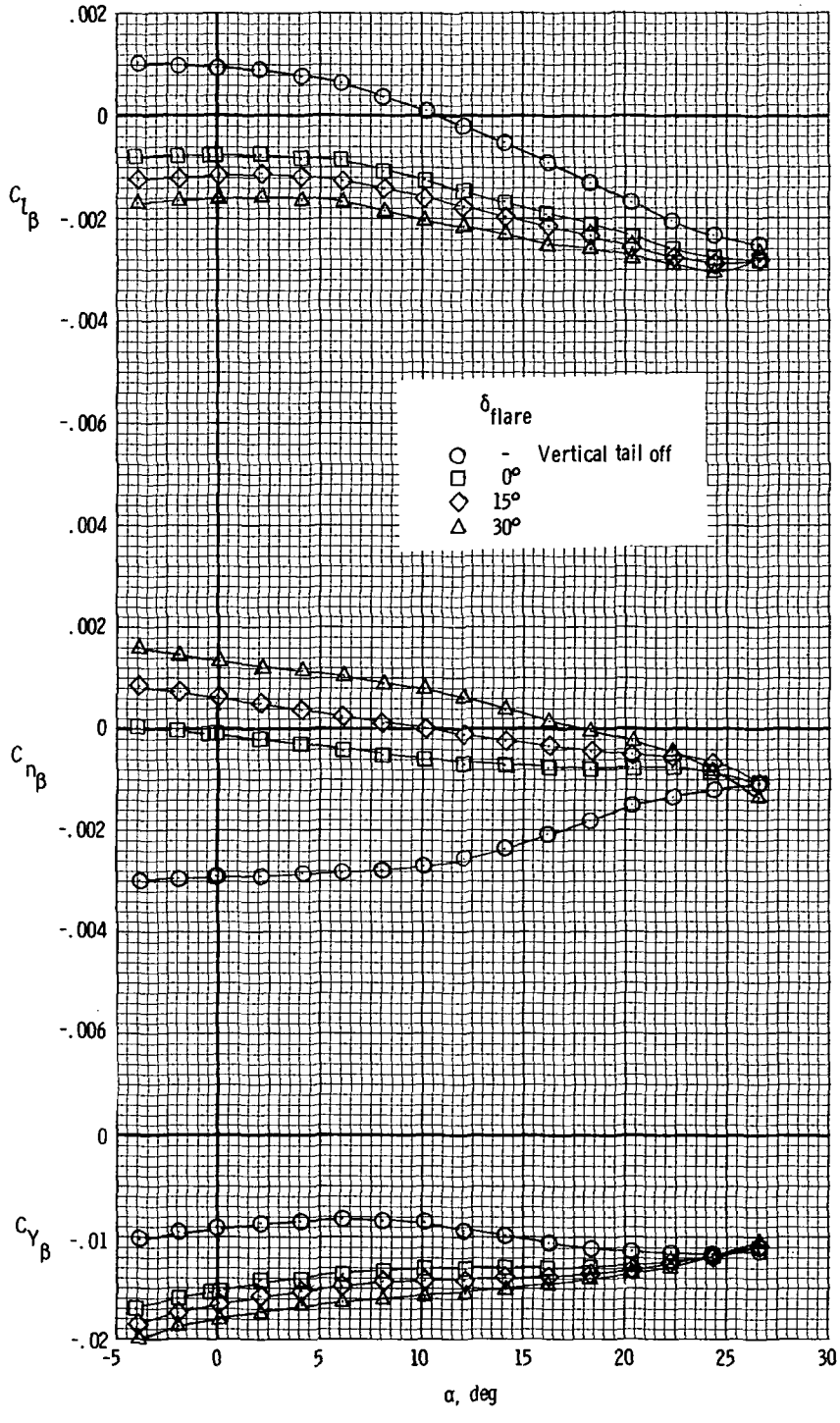

(c) Lateral and directional stability derivatives.

Figure 9.- Concluded.

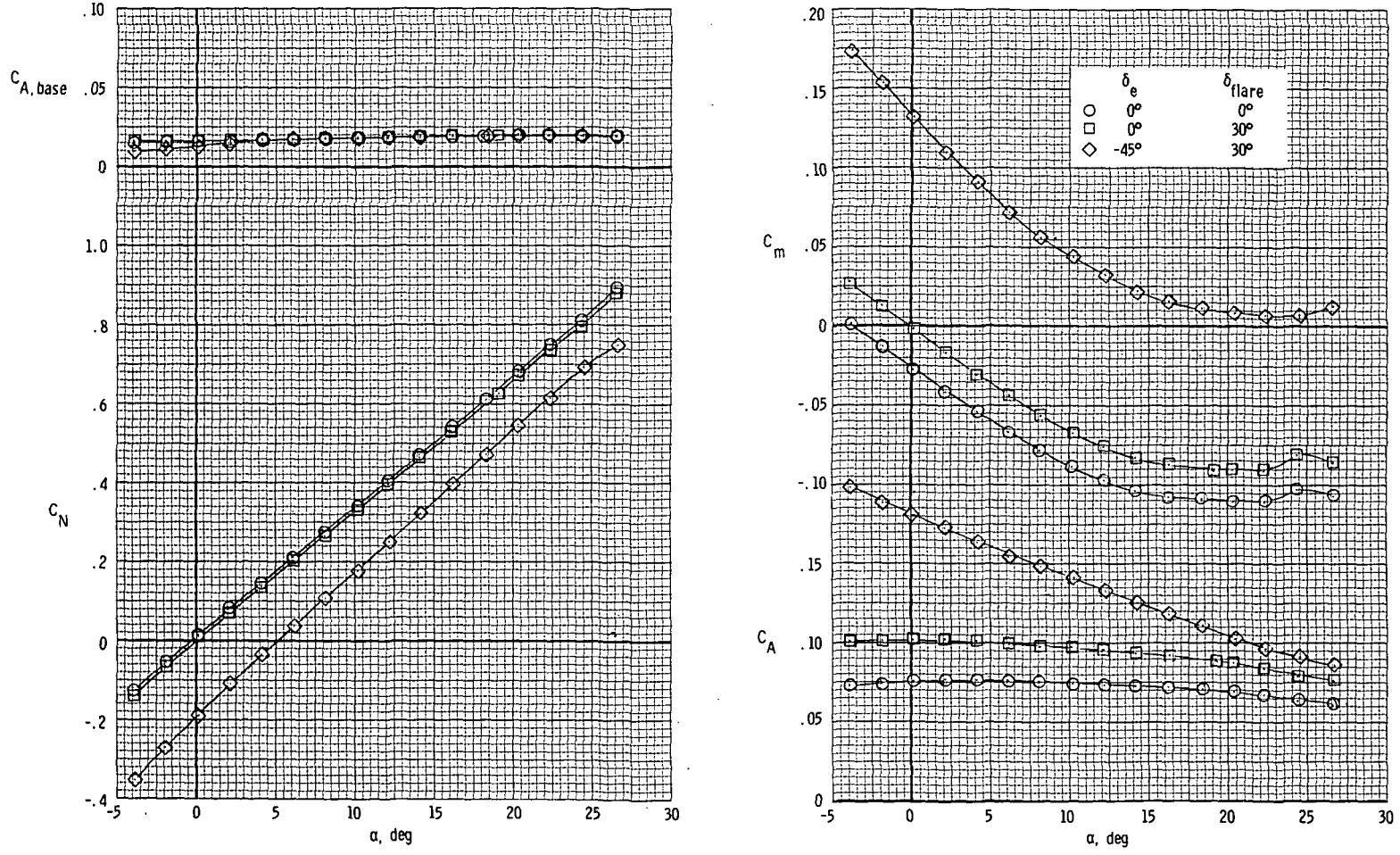

(a) Body-axis data.

Figure 10.- Effects of the flared rudder and elevon deflection on the aerodynamic characteristics of the configuration with orbital-maneuvering-system fairing and $\delta_r = 0^o$.

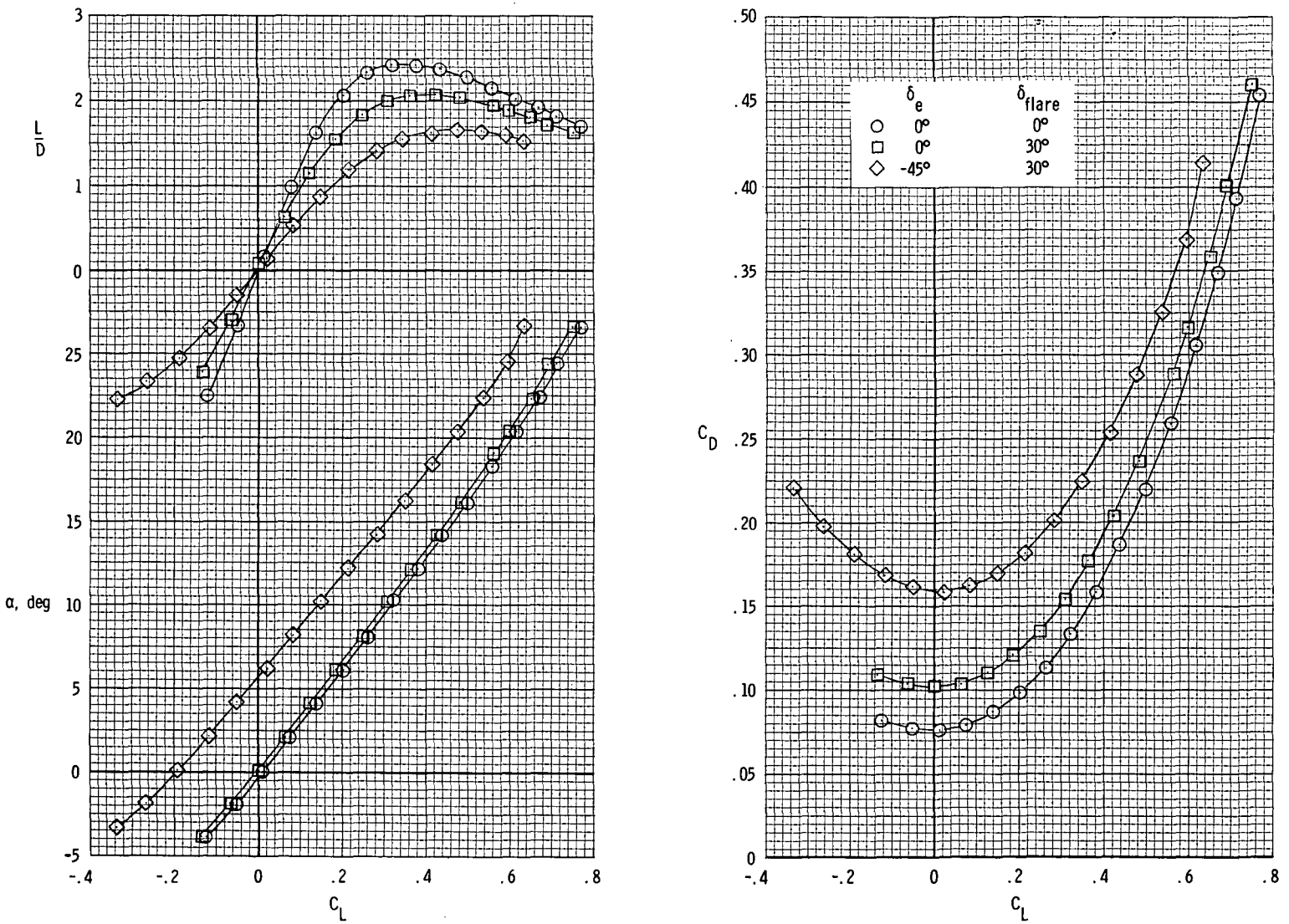

(b) Stability-axis data.

Figure 10.- Continued.

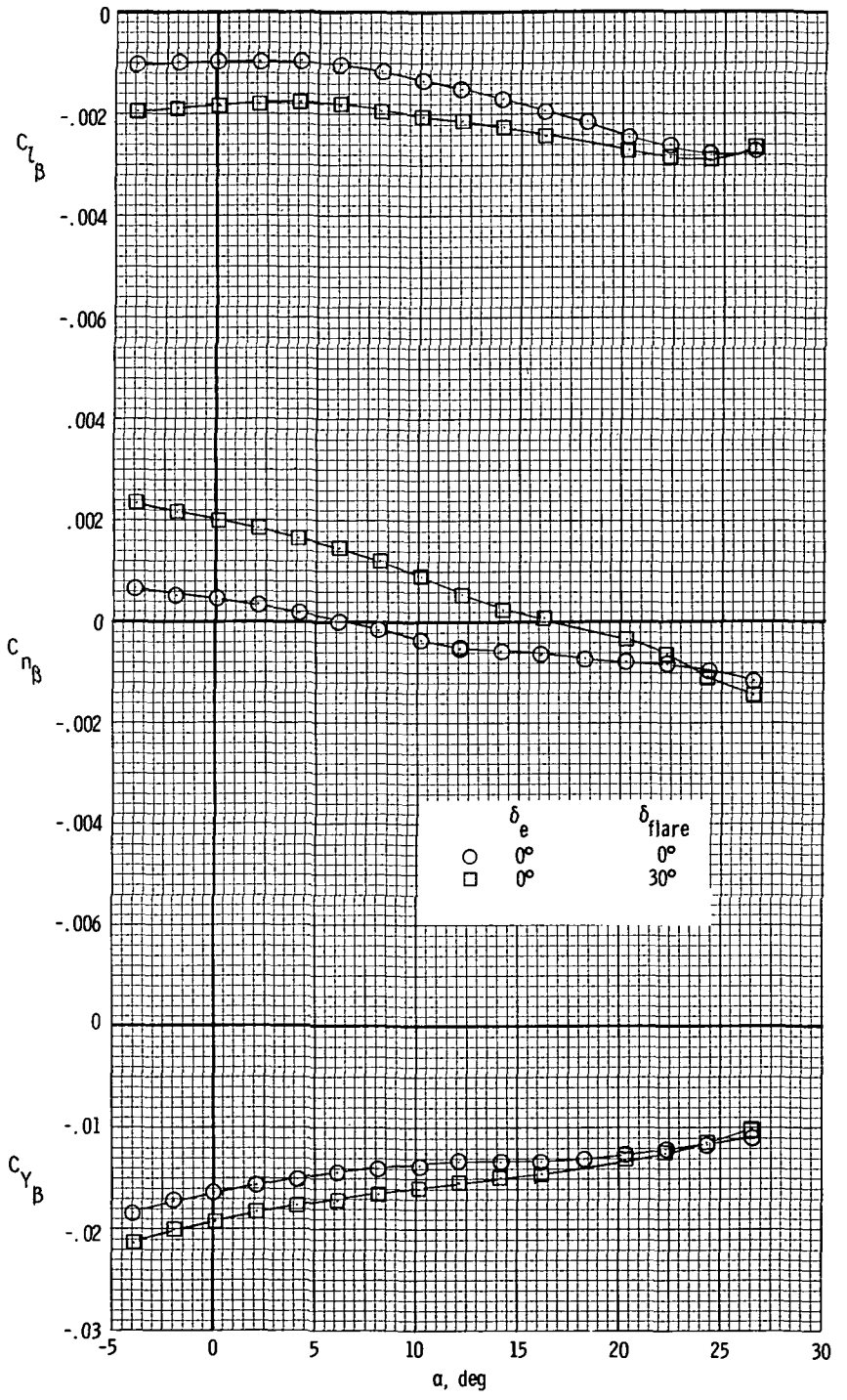

(c) Lateral and directional stability derivatives.

Figure 10.- Concluded.

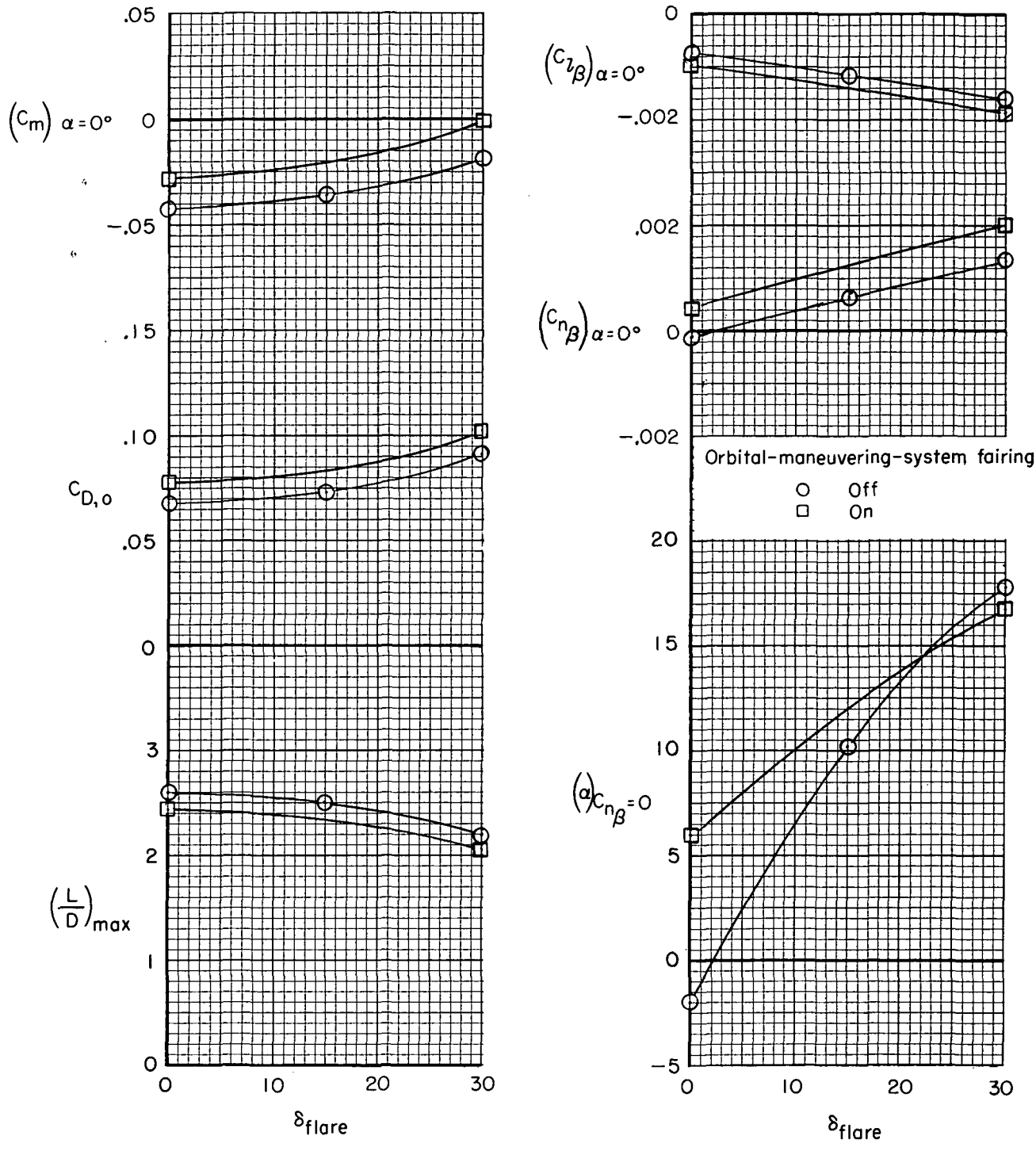

Figure 11.- Summary of the effects of rudder flare angle on the aerodynamic characteristics of the configuration. Symbols denote quantities obtained from faired curves.

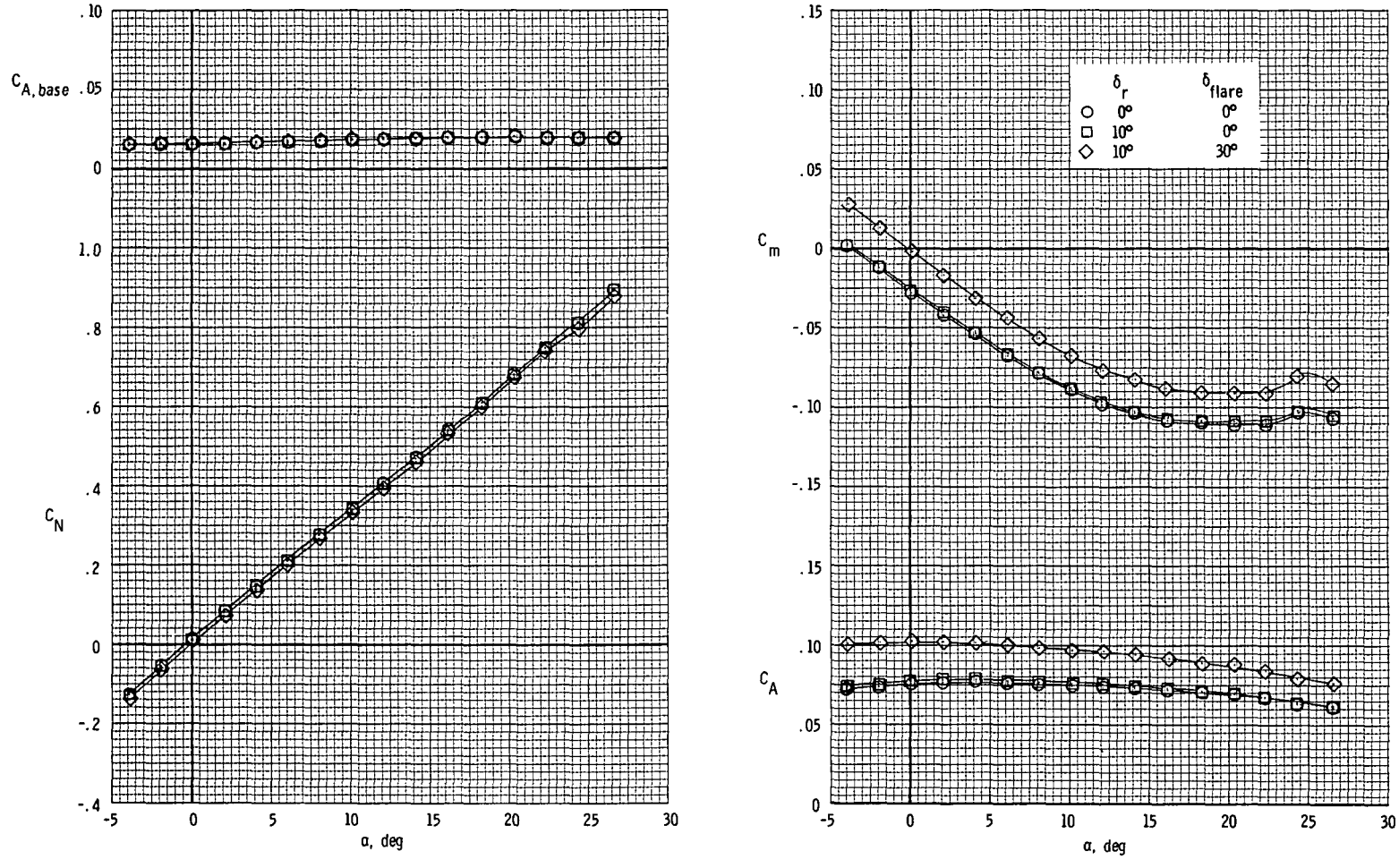

(a) Body-axis data.

Figure 12.- Effects of rudder deflection on the aerodynamic characteristics of the configuration with orbital-maneuvering-system fairing and $\delta_e = 0^o$.

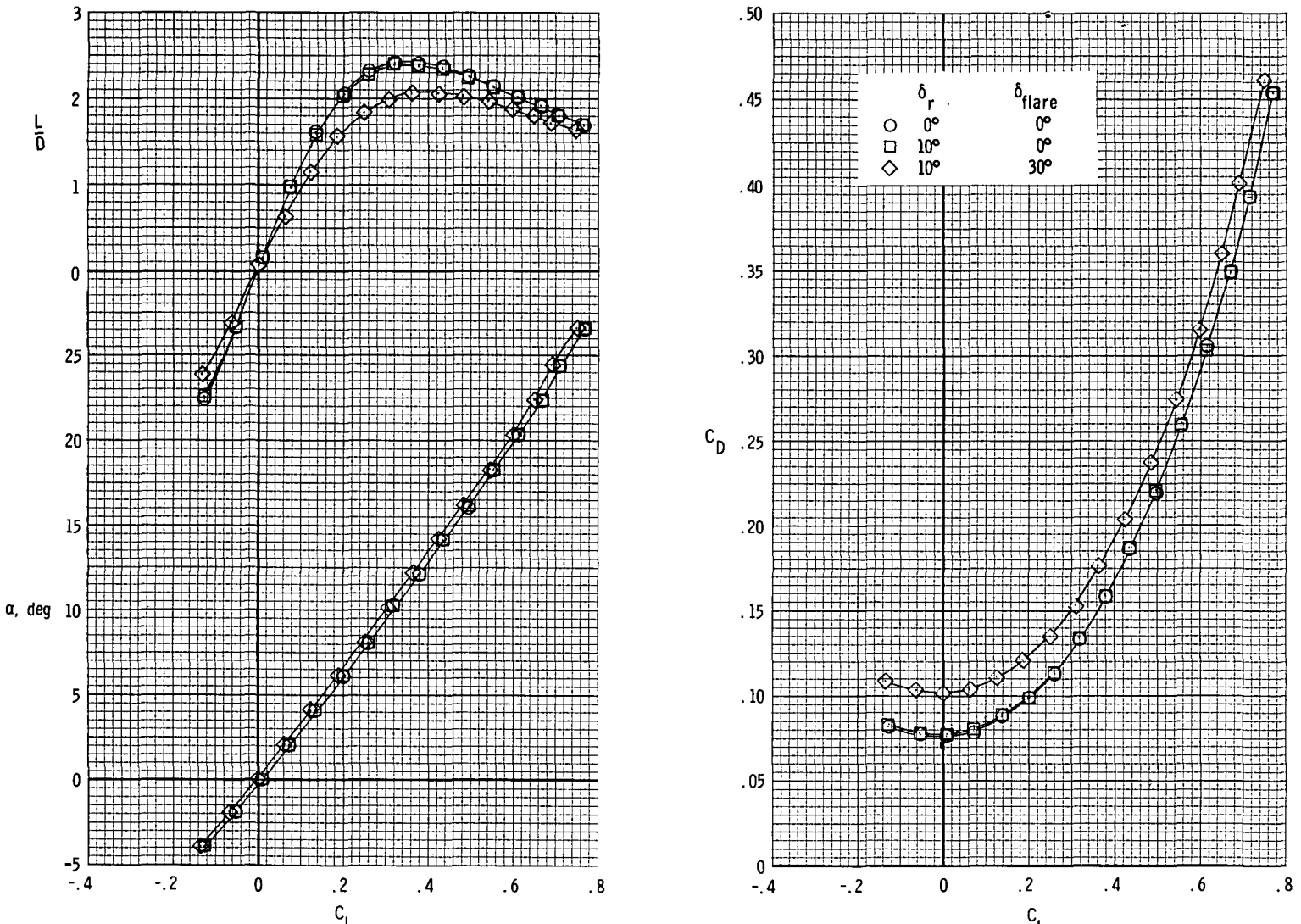

(b) Stability-axis data.

Figure 12.- Concluded.

"The aeronautical and space activities of the United States shall be conducted so as to contribute . . . to the expansion of human knowledge of phenomena in the atmosphere and space. The Administration shall provide for the widest practicable and appropriate dissemination of information concerning its activities and the results thereof."

—NATIONAL AERONAUTICS AND SPACE ACT OF 1958

NASA SCIENTIFIC AND TECHNICAL PUBLICATIONS

TECHNICAL REPORTS: Scientific and technical information considered important, complete, and a lasting contribution to existing knowledge.

TECHNICAL NOTES: Information less broad in scope but nevertheless of importance as a contribution to existing knowledge.

TECHNICAL MEMORANDUMS: Information receiving limited distribution because of preliminary data, security classification, or other reasons.

CONTRACTOR REPORTS: Scientific and technical information generated under a NASA contract or grant and considered an important contribution to existing knowledge.

TECHNICAL TRANSLATIONS: Information published in a foreign language considered to merit NASA distribution in English.

SPECIAL PUBLICATIONS: Information derived from or of value to NASA activities. Publications include conference proceedings, monographs, data compilations, handbooks, sourcebooks, and special bibliographies.

TECHNOLOGY UTILIZATION PUBLICATIONS: Information on technology used by NASA that may be of particular interest in commercial and other non-aerospace applications. Publications include Tech Briefs, Technology Utilization Reports and Technology Surveys.

Details on the availability of these publications may be obtained from:

SCIENTIFIC AND TECHNICAL INFORMATION OFFICE

NATIONAL AERONAUTICS AND SPACE ADMINISTRATION

Washington, D.C. 20546